Eva Morava
Matthias Baumgartner
Marc Patterson
Shamima Rahman
Johannes Zschocke
Verena Peters *Editors*

JIMD Reports

Volume 34

SSIEM

Springer

JIMD Reports
Volume 34

Eva Morava
Editor-in-Chief

Matthias Baumgartner · Marc Patterson · Shamima Rahman · Johannes Zschocke
Editors

Verena Peters
Managing Editor

JIMD Reports
Volume 34

Springer

SSIEM

ISSN 2192-8304 ISSN 2192-8312 (electronic)
JIMD Reports
ISBN 978-3-662-55585-9 ISBN 978-3-662-55586-6 (eBook)
DOI 10.1007/978-3-662-55586-6

This Springer imprint is published by Springer Nature
The registered company is Springer-Verlag GmbH Germany
The registered company address is: Heidelberger Platz 3, 14197 Berlin, Germany

Contents

Diaphragmatic Eventration in Sisters with Asparagine Synthetase Deficiency: A Novel Homozygous *ASNS* Mutation and Expanded Phenotype 1
Jun Sun, Angela J McGillivray, Jason Pinner, Zhihui Yan, Fengxia Liu, Drago Bratkovic, Elizabeth Thompson, Xiuxiu Wei, Huifeng Jiang, Asan, and Maya Chopra

Measurement of Elevated Concentrations of Urine Keratan Sulfate by UPLC-MSMS in Lysosomal Storage Disorders (LSDs): Comparison of Urine Keratan Sulfate Levels in MPS IVA Versus Other LSDs 11
Katarzyna A. Ellsworth, Laura M. Pollard, Sara Cathey, and Tim Wood

The Spectrum of PAH Mutations and Increase of Milder Forms of Phenylketonuria in Sweden During 1965–2014 19
Annika Ohlsson, Helene Bruhn, Anna Nordenström, Rolf H. Zetterström, Anna Wedell, and Ulrika von Döbeln

DMP1-CDG (CDG1e) with Significant Gastrointestinal Manifestations; Phenotype and Genotype Expansion 27
C. Bursle, D. Brown, J. Cardinal, F. Connor, S. Calvert, and D. Coman

Classical Galactosaemia and CDG, the N-Glycosylation Interface. A Review 33
Ashwini Maratha, Hugh-Owen Colhoun, Ina Knerr, Karen P. Coss, Peter Doran, and Eileen P. Treacy

Argininosuccinic Acid Lyase Deficiency Missed by Newborn Screen 43
Rebecca D. Ganetzky, Emma Bedoukian, Matthew A. Deardorff, and Can Ficicioglu

Very Long-Chain Acyl-Coenzyme A Dehydrogenase Deficiency and Perioperative Management in Adult Patients 49
M.M. Welsink-Karssies, J.A.W. Polderman, E.J. Nieveen van Dijkum, B. Preckel, W.S. Schlack, G. Visser, C.E. Hollak, and J. Hermanides

Paracentric Inversion of Chromosome 21 Leading to Disruption of the *HLCS* Gene in a Family with Holocarboxylase Synthetase Deficiency 55
Shane C. Quinonez, Andrea H. Seeley, Cindy Lam, Thomas W. Glover, Bruce A. Barshop, and Catherine E. Keegan

Delayed Infusion Reactions to Enzyme Replacement Therapies 63
Zahra Karimian, Chester B. Whitley, Kyle D. Rudser, and Jeanine R. Jarnes Utz

Novel *PEX3* Gene Mutations Resulting in a Moderate Zellweger Spectrum Disorder 71
C. Maxit, I. Denzler, D. Marchione, G. Agosta, J. Koster, R.J.A. Wanders, S. Ferdinandusse, and H.R. Waterham

Improved Measurement of Brain Phenylalanine and Tyrosine Related to Neuropsychological Functioning in Phenylketonuria 77
Susan E. Waisbren, Sanjay P. Prabhu, Patricia Greenstein, Carter Petty, Donald Schomer, Vera Anastasoaie, Kalin Charette, Daniel Rodriguez, Sai Merugumala, and Alexander P. Lin

Table of Phenylalanine Content of Foods: Comparative Analysis of Data Compiled in Food Composition Tables 87
Ana Claudia Marquim F. Araújo, Wilma M. C. Araújo, Ursula M. Lanfer Marquez, Rita Akutsu, and Eduardo Y. Nakano

Inhaled Sargramostim Induces Resolution of Pulmonary Alveolar Proteinosis in Lysinuric Protein Intolerance 97
Laura M. Tanner, Johanna Kurko, Maaria Tringham, Heikki Aho, Juha Mykkänen, Kirsti Näntö-Salonen, Harri Niinikoski, and Heikki Lukkarinen

COXPD9 an Evolving Multisystem Disease; Congenital Lactic Acidosis, Sensorineural Hearing Loss, Hypertrophic Cardiomyopathy, Cirrhosis and Interstitial Nephritis 105
C. Bursle, A. Narendra, R. Chuk, J. Cardinal, R. Justo, B. Lewis, and D. Coman

Incidence and Geographic Distribution of Succinic Semialdehyde Dehydrogenase (SSADH) Deficiency 111
Savita Verma Attri, Pratibha Singhi, Natrujee Wiwattanadittakul, Jyotindra N. Goswami, Naveen Sankhyan, Gajja S. Salomons, Jean-Baptiste Roullett, Ryan Hodgeman, Mahsa Parviz, K. Michael Gibson, and Phillip L. Pearl

JIMD Reports
DOI 10.1007/8904_2016_3

CASE REPORT

Diaphragmatic Eventration in Sisters with Asparagine Synthetase Deficiency: A Novel Homozygous *ASNS* Mutation and Expanded Phenotype

Jun Sun · Angela J McGillivray · Jason Pinner · Zhihui Yan · Fengxia Liu · Drago Bratkovic · Elizabeth Thompson · Xiuxiu Wei · Huifeng Jiang · Asan · Maya Chopra

Received: 15 March 2016 / Revised: 14 June 2016 / Accepted: 15 June 2016 / Published online: 27 July 2016

Abstract *Background*: Asparagine Synthetase Deficiency (ASNSD; OMIM #615574) is a newly described rare autosomal recessive neurometabolic disorder, characterised by congenital microcephaly, severe psychomotor delay, encephalopathy and progressive cerebral atrophy. To date, seven families and seven missense mutations in the ASNSD disease causing gene, *ASNS*, have been published. *Methods*: We report two further affected infant sisters from a consanguineous Indian family, who in addition to the previously described features had diaphragmatic eventration. Both girls died within the first 6 months of life. Whole exome sequencing (WES) was performed for both sisters to identify the pathogenic mutation. The clinical and biochemical parameters of our patient are compared to previous reports. *Results*: WES demonstrated a homozygous novel missense *ASNS* mutation, c.1019G > A, resulting in substitution of the highly conserved arginine residue by histidine (R340H). *Conclusion*: This report expands the phenotypic and mutation spectrum of ASNSD, which should be considered in neonates with congenital microcephaly, seizures and profound neurodevelopmental delay. The presence of diaphragmatic eventration suggests extracranial involvement of the central nervous system in a disorder that was previously thought to exclusively affect the brain. Like all previously reported patients, these cases were diagnosed with WES, highlighting the clinical utility of next generation sequencing in the diagnosis of rare, difficult to recognise disorders.

Communicated by: Verena Peters

Competing interests: None declared

Please note that Jun Sun and Angela J. McGillivray contributed equally and should be shared first authors. Maya Chopra and Asan should be co-corresponding authors.

Electronic supplementary material: The online version of this chapter (doi:10.1007/8904_2016_3) contains supplementary material, which is available to authorized users.

J. Sun · F. Liu · X. Wei · Asan (✉)
Binhai Genomics Institute, BGI-Tianjin, BGI-Shenzhen, Tianjin 300308, China
e-mail: asan@genomics.cn

J. Sun · F. Liu · X. Wei · Asan
Tianjin Enterprise Key Laboratory of Clinical molecular diagnostic, BGI-Shenzhen, Tianjin 300308, China

J. Sun · F. Liu · X. Wei · Asan
BGI-Shenzhen, Shenzhen 518083, China

A.J. McGillivray
Department of Newborn Care, Royal Prince Alfred Hospital, Missenden Road, Camperdown, 2050 Sydney, NSW, Australia

J. Pinner · M. Chopra (✉)
Department of Medical Genomics, Royal Prince Alfred Hospital, Missenden Road, Camperdown, 2050 Sydney, NSW, Australia
e-mail: Maya.Chopra@sswahs.nsw.gov.au

Z. Yan · H. Jiang
Key Laboratory of Systems Microbial Biotechnology, Tianjin Institute of Industrial Biotechnology, Chinese Academy of Sciences, Tianjin 300308, China

D. Bratkovic
Metabolic Clinic, South Australian Clinical Genetics Service, SA Pathology, 5000 Adelaide, SA, Australia

E. Thompson
Department of Radiology, Royal Prince Alfred Hospital, Missenden Road, Camperdown, Sydney 2050 NSW, Australia

M. Chopra
Shanghai First Maternity and Infant Hospital, Tongji University School of Medicine, Shanghai, China

M. Chopra
Discipline of Genetic Medicine, University of Sydney, Sydney 2050, NSW, Australia

Introduction

Asparagine Synthetase Deficiency (ASNSD) was first described in 2013 as a rare autosomal recessive inborn error of non-essential amino acid synthesis caused by homozygous or compound heterozygous mutations in the *ASNS* gene (Ruzzo et al. 2013). In the initial report of nine individuals from four families, key features included: congenital microcephaly, intellectual disability, progressive cerebral atrophy and early onset intractable seizures. Recently, four additional patients from three families were reported (Ben-Salem et al. 2015; Alfadhel et al. 2015; Palmer et al. 2015). The *ASNS* gene is highly expressed in the brain and encodes for asparagine synthetase, the enzyme which catalyses the ammonia transfer from glutamine to aspartic acid (Ruzzo et al. 2013). While CSF and plasma amino acid profiles may be abnormal in ASNSD, normal levels have been seen in some patients, making biochemical diagnosis unreliable and contributing to the challenge in diagnosing this rare disorder.

We report two sisters, born to consanguineous parents (first cousins) of Indian ancestry, with ASNSD caused by a novel missense homozygous mutation in *ASNS*. This is now the eighth family to be reported with this disorder, and the eighth pathogenic mutation. We describe the phenotypic, biochemical and molecular features of our two patients and compare them with previously reported cases.

Clinical Report

We report on two affected sisters born to first cousin Indian parents (see Fig. 1a).

Patient 1

Patient 1 was born at 38 weeks' gestation following a pregnancy complicated by intrauterine growth restriction. Her birth weight was 2,216 g, length 45.5 cm and OFC 30.5 cm (all less than 3rd percentile). She had flattened and simple ears and a prominent nasal tip. Following an episode of aspiration, she was found to have elevation of the right hemidiaphragm on chest X-ray. Airway fluoroscopy demonstrated paradoxical movement on the right side consistent with phrenic nerve palsy and eventration. She underwent two right-sided hemidiaphragmatic plications. She had progressive respiratory failure due to diaphragmatic failure followed by central respiratory failure. She became dependent on nasogastric feeds and her growth remained static. She was jittery and had early truncal hypotonia, then generalised hypertonia with clonus. There were no seizures. Cerebral MRI at 3 weeks showed mild ventriculomegaly, simplified gyral pattern, and hypoplasia of the pons and cerebellum and mild delay in myelination. At 3 months there was cortical volume loss, corpus callosum thinning and bilateral caudate atrophy. EEG at 3 weeks showed low voltage with no epileptiform activity. At 3 months EEG was very abnormal with episodic bursts of theta, delta and sharp activity with an intervening isoelectric pattern. She became dependent on ventilator support. Critical care was withdrawn at 6 months of age.

Patient 2

Patient 2 was born 7 years after Patient 1. Two healthy boys were born in the intervening period. She was born at 37 weeks and 5 days by caesarean section following reduced foetal movements and abnormal cardiotocography (CTG). Intrauterine growth restriction with severe microcephaly was noted prenatally. Her birth weight was 2,236 g, length 44.5 cm and head circumference 28.5 cm (all <3rd percentile). Respiratory insufficiency was present from birth, requiring intubation and ventilation. She had a sloping forehead, hypertelorism and a prominent nasal tip. She had hyperekplexia but no evidence of clinical seizures. Amp-integrated Brainz EEG demonstrated a premature pattern but there were no electrical seizures. She initially had hypertonia and hyperreflexia, which evolved into hypotonia and minimal gag reflex. Cerebral MRI on day 5 showed a simplified gyral pattern, mild ventriculomegaly with enlarged axial spaces, suggesting a moderate degree of atrophy and hypoplasia of the corpus callosum, pons and inferior cerebellum (see Fig. 1b–g). Myelination was age-appropriate. She developed right-sided diaphragmatic eventration (see Fig. 1h), with associated refractory lung collapse, diminishing respiratory effort and three failed extubation attempts. She had right-sided choanal stenosis. She died on day 11.

Methods

Preliminary Investigations

See supplementary information.

Homozygosity Mapping in Patient 2

The determination of long segments of chromosome homozygosity (LSCH) in Patient 2 was performed with single nucleotide polymorphism (SNP) analysis using an Illumina HuamnCore-12 v1.0 array (mean resolution 0.2 Mb).

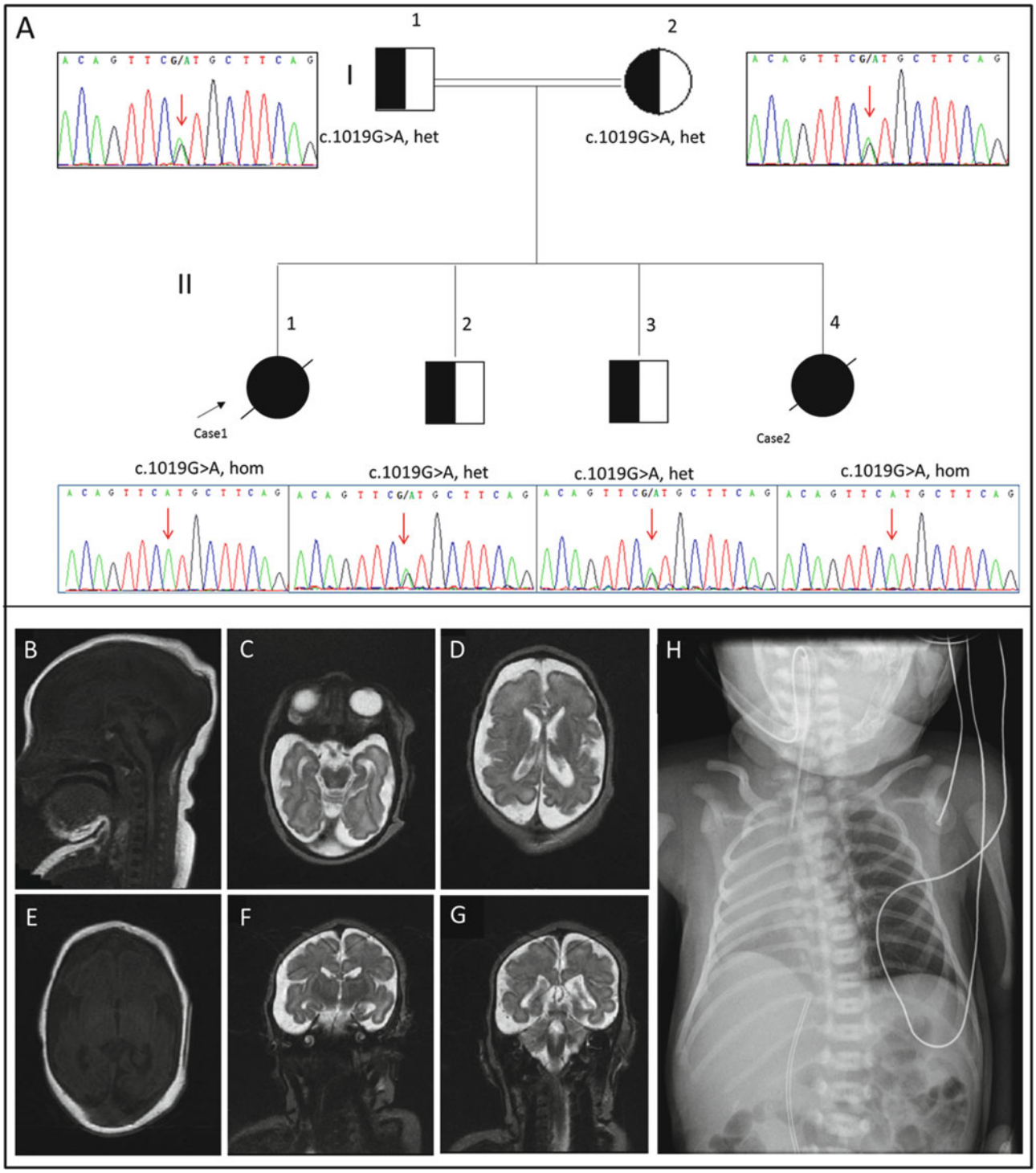

Fig. 1 (**A**) Pedigree and chromatograms of the DNA sequence changes in *ASNS*. The parents and siblings are heterozygous for the c.1019G > A variant. Patients 1 and 2 are homozygous for this variant. (**B**–**G**) MRI brain of Patient 2 at 5 days old. B Sagittal T1 demonstrates small corpus callosum, atrophic brainstem and vermis. C&D Axial T2 images show severe microcephaly and prominence of the lateral ventricles, particularly the temporal horns. E Axial T1 shows wide Sylvian fissure and prominent subarachnoid space overlying the small cerebral hemispheres. F Coronal T2 shows generalised microcephaly, with severe involvement of the temporal lobes. G Coronal T2 demonstrates enlarged trigones of both lateral ventricles. (**H**) Chest X-ray of Patient 2, showing raised right hemidiaphragm and midline mediastinal shift to the right

Exome Sequencing

Whole exome sequencing (WES) was performed on two affected subjects by BGI, Shenzhen, China (see supplementary information).

Data Analysis

Raw data was processed by the Illumina pipeline (version 1.3.4) for image analysis, error estimation, base calling and generation of the primary sequence data. A local algorithm was used to remove low-quality reads and potential adaptor contamination from the primary data. The called variants were annotated using Gaea, a BGI in-house developed annotation pipeline. The details of data analysis are described in the supplementary information.

Variant Interpretation

Given the history of consanguinity in the family, homozygosity mapping followed by exome sequencing was implemented. Variants identified by exome sequencing were filtered based on their annotated function and allele frequency in control databases. We then focussed on the subset of the filtered variants which were identified within LSCH. The associated phenotypic features of candidate genes were analysed against the patient's phenotype. The phenotype match was based on the OMIM database (http://omim.org/) and published papers.

Sanger Sequencing

The identified possible disease causing mutation in *ASNS* was confirmed as homozygous by Sanger sequencing for two patients and as heterozygous in unaffected family members (parents and two unaffected brothers).

Molecular Dynamics Simulation

A workspace of automated homology modelling, SWISS-MODEL (Biasini et al. 2014), was used to construct the 3D structure of ASNS and mutant R340H from homo sapiens (amino acid sequence NP_899199). By alignment, the structure of asparagine synthetase B (ASNB) from E. coli (Larsen et al. 2000) was selected as the template to construct the model as it shares a sequence identity of ~49% with the human ASNS sequence.

See supplementary information.

Results

Patient 1

Initial normal genetic investigations included 400 band resolution G-banding metaphase karyotype, 17p13.2 (*LIS1*) florescent in situ hybridisation and subtelomere multiligand probe amplification. Metabolic investigations showed normal urine amino and organic acids, serum ammonia, creatine kinase, orotic acid, very long chain fatty acids, cholesterol, 7-dehydrocholesterol, transferrin isoforms and cerebrospinal fluid (CSF) pyruvate, glucose, protein, lactate and amino acids. While serum and CSF amino acids were reported as normal, neither included analysis of asparagine. Serology provided no evidence for prior infection with cytomegalovirus, toxoplasmosis, rubella or syphilis.

Patient 2

Initial genetic investigations included a normal oligonucleotide chromosome array, and an SNP array which did not detect any clinically significant genomic imbalance but identified 20 long continuous stretches of homozygosity on chromosomes 2, 5, 7, 8, 9, 10, 12, 16 and 18, representing 8.6% of the genome (see supplementary information). Metabolic investigations showed normal urinary organic and amino acids and glycosaminoglycans, plasma very long chain fatty acids, 7-dehydrocholesterol and transferrin isoforms. Plasma amino acids detected low asparagine (7 μmol/L, reference range 26–76 μmol/L) and cystine levels (19 μmol/L, reference range 28–77 μmol/L). CSF amino acid analysis was not performed.

Whole Exome Sequencing

WES was performed for the two affected daughters in this family. For Patient 2, for whom an adequate DNA sample was available, 9,570 megabases of raw data was generated with a depth of 98.11-fold for the target region. For Patient 1, the quantity was insufficient for standard WES library construction. Only 4,009 megabases of raw data was generated with a depth of 32.87-fold for the target region for Patient 1 (see supplementary information).

Because of concerns of inadequate coverage in Patient 1, primary analysis focussed on Patient 2. The list of candidate genes from Patient 2 was then compared manually with Patient 1.

In total, 25,232 variants were identified in Patient 2, of which 10,217 were in regions of LSCH. After filtering out those variants which were synonymous, non-coding or present in >1% of population according to internal and public databases, 62 variants remained of which 19 were homozygous. These 19 homozygous variants were then manually compared to Patient 1. There was at least 10× coverage in Patient 1 for 18 of the 19 sites. The one variant that was not covered well in Patient 1 was in the *FMNL2* gene, which is not known to be disease causing. Of the 19 homozygous variants in Patient 2, 11 were also homozygous in Patent 1.

Identification of Pathogenic Mutation

The 19 variants remaining after filtration were interpreted manually according to phenotype, function, site conservation and software prediction (supplementary information). Of the 19 homozygous variants identified in Patient 2, two were predicted to be deleterious by PolyPhen2 software (Adzhubei et al. 2010) and Ens Condel software (Gonzalez-Perez and Lopez-Bigas 2011), and only one of these two variants, a missense variant in the *ASNS* gene (c.1019G > A), was also identified in Patient 1 in homozygous form. The c.1019G > A in the *ASNS* gene was absent in the four control databases used in this analysis. Given the consistent clinical, neuro-imaging and biochemical phenotype, this homozygous mutation in the *ASNS* gene (c.1019G > A) was determined to be the disease causing mutation in this family. We found that most reported pathogenic *ASNS* mutations are located in the same domain as the mutation identified in our patients (see Fig. 2a).

The missense mutation c.1019G > A in the *ASNS* gene results in substitution of the highly conserved arginine residue by histidine at position 340 (see Fig. 2b). Sanger validation of this mutation was performed on all family members. The parents and brothers were found to be heterozygous for the mutation (see Fig. 1), which is consistent with the autosomal recessive inheritance mode of ASNSD.

Molecular Dynamics Simulation

We constructed a protein model of human ASNS based on the structure of ASNB from *E. coli*. According to the sequence alignment, position R340 in human ASNS corresponds to R324 in *E. coli* ASNB, and this residue is highly conserved (Supplementary Fig. 1). The protein structure of human ASNS was modelled according to the structure of ASNB (Fig. 2c). The topology of the two proteins, human ASNS (brown) and *E. coli* ASNB (blue), are very similar, except for the unstable loop regions (Fig. 2c). From the structural alignment, we found that the highly conserved position 340 is very close to the catalytic activity centre. Indeed, when arginine at the corresponding position in *E. coli* was substituted by alanine, leucine or lysine, the Asn synthetase activity disappeared (Richards and Schuster 1998). It is possible that the mutation from arginine to histidine also affects the enzyme activity of ASNS in humans.

We also performed molecular dynamics (MD) simulation on wild type (WT) and mutant R340H. The details of this experiment are in the supplementary information. We demonstrated that the R340 mutation results in a protein which is less compact.

Discussion

We describe two infant sisters with congenital microcephaly, severe psychomotor retardation and cortical and posterior fossa atrophy in whom WES identified a novel pathogenic homozygous *ASNS* mutation, c.1019G > A, p.R340H. This variant was absent in public and internal databases, predicted to be pathogenic on in silico analysis and confirmed on Sanger sequencing. The parents and unaffected siblings were confirmed as heterozygous for the mutation. Furthermore, reduced plasma asparagine in Patient 2 provided further evidence of a phenotypic consequence for the mutation. With these additional two cases, there are now 15 published patients with homozygous or compound heterozygous mutations in *ASNS* resulting in ASNSD, a newly described very rare neurometabolic disorder.

The *ASNS* gene maps to chromosome 7, spans 35 kb and contains 13 exons (Zhang et al. 1989). The enzyme asparagine synthetase converts aspartate to asparagine, with glutamine as the amino donor group in an ATP-dependent reaction (Alfadhel et al. 2015; Zhang et al. 1989).

The in-silico model of the mutant ASNS protein shows that the highly conserved position 340 is adjacent to the catalytic region, therefore substitution of arginine residue by histidine at this position may have a significant effect on the enzyme reaction.

The R340H mutation is in the C-terminal domain of the ASNS enzyme, and most reported pathogenic mutations are located in the same domain. In 3D modelling, the change is near the ATP binding pocket, in common with the majority of *ASNS* mutations reported to date (Palmer et al. 2015). Mutations in these regions may alter ATP binding or hydrolysis (Palmer et al. 2015).

There is enrichment of *ASNS* expression in foetal mouse brain, in patterns similar to those seen in the primary microcephaly genes (Ruzzo et al. 2013; Bond et al. 2002; Jackson et al. 2002). The hypomorphic *Asns* mouse model

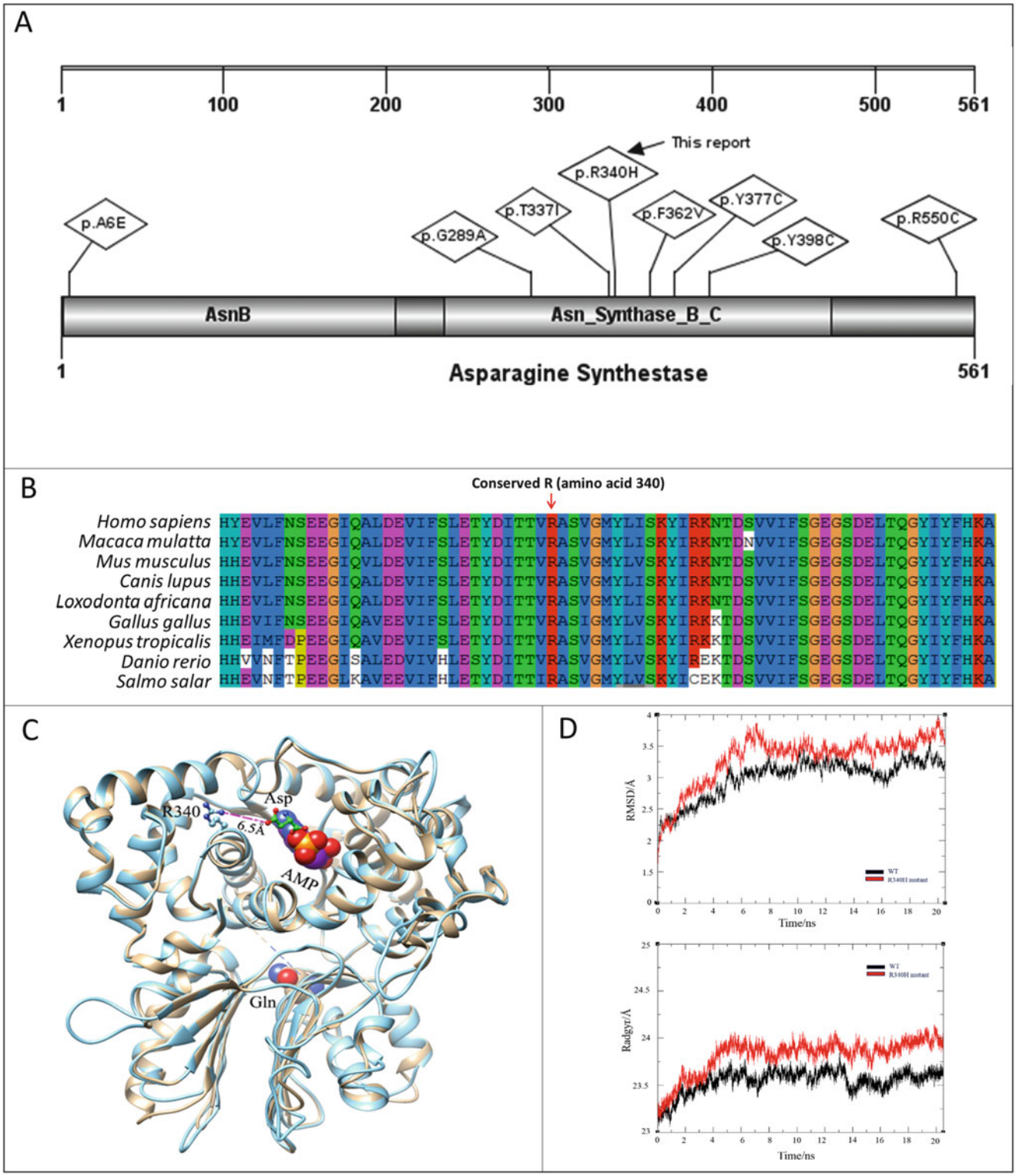

Fig. 2 (**A**) Allelic spectrum and location by functional domain of reported pathogenic mutations of the *ASNS* gene. The R340H mutation identified in this study is marked with a *black arrow*. (**B**) Evolutionary sequence conservation analysis. Multiplex sequence alignment of the ASNS protein across ten different species from *homo sapiens* to *Salmo salar* shows that Arginine (R) at codon 340 is highly conserved among species. The *red arrow* locates codon 340 of the ASNS protein. (**C**) ASNS and asnB ASNB structure. The E. coli ASNB is shown in *blue*. (**D**) Molecular dynamics simulations on wild type and mutant R340H ASNS protein. The *black curve* denotes the structural dynamics of the WT protein and the *red curve* denotes the R340H protein. The root square deviation of backbone atoms (RMSD) reflects a stable protein, allowing for comparison of structure. Radgyr (radius of gyration) reflects the volume of protein structure. The higher Radgyr value in the *red curve* suggests that the mutant protein is held in a more extended state